Eur. Phys. J. D **37**, 361–369 (2006)
DOI: 10.1140/epjd/e2005-00305-4

THE EUROPEAN PHYSICAL JOURNAL D

Modified Kolbensvedt model for the electron impact K-shell ionization cross-sections of atoms and ions

M.A. Uddin[1,a], A.K.F. Haque[1], K.R. Karim[2], A.K. Basak[1], and F.B. Malik[3,4]

[1] Department of Physics, University of Rajshahi, Rajshahi, Bangladesh
[2] Department of Physics, Department of Physics, Illinois State University, Normal, IL 61790, USA
[3] Department of Physics, Southern Illinois University, Carbondale, IL 62901, USA
[4] Department of Physics, Washington University, St. Louis, Mo 63130, USA

Received 15 July 2005/ Received in final form 27 September 2005
Published online 16 November 2005 –

Abstract. A modification of the Kolbensvedt model, MKLV, in terms of ionic, correlation (between the incident and target electrons) and relativistic corrections, is proposed to calculate the K-shell electron impact ionization cross-sections of neutral and ionic targets. The modified model, with a single set of parameters, is found to reproduce satisfactorily the experimental data for the neutral H, Al, Ar, Mn, Ge, Mo, Ag, Sn, Au, Bi and U and ionic Li^+, B^{4+} and O^{7+} targets better than the existing empirical models from threshold energies to as high as 10^4 MeV. For the Ag target, the calculations from MKLV follow closely the results of Scofield, and for Au, those of Scofield, and Ndefru and Malik, both done in the relativistic Born approximation with the Møller interaction, at energies higher than the peak region.

PACS. 34.80.Dp Atomic excitation and ionization by electron impact

1 Introduction

The information on K-shell ionization cross-sections by electron impact is necessary for doing quantitative analyses of data in many fields of physics such as Auger-electron spectroscopy, electron probe microanalysis and electron energy loss spectroscopy. They are also needed for various purposes in astrophysics, atmospheric physics, radiation and plasma physics. Aside from these applications, the study of the electron impact ionization process is of fundamental interest in the understanding of atomic reaction mechanism, collision dynamics, and the role of quantum electrodynamics in determining electron-electron interaction.

The available experimental data are still far from being adequate to meet the increasing demands in the applications. Moreover, very often than not, significant discrepancies amongst data from different sources exist reflecting considerable difficulties and uncertainties involved in cross-section measurements. This situation underscores the importance and need for providing cross-section information data by the theoretical methods. The ab-initio quantum mechanical methods quite often provide accurate cross-sections. Unfortunately, such calculations for electron-impact ionization cross-sections (EIICS) from the first principles have only been done in a few cases.

A detailed quantum mechanical calculation of EIICS is, in principle, feasible but in practice, it involves many-body reaction mechanism and leads to many approximations, the most common ones being the distorted wave Born approximation (DWBA) [1] and coupled channel approximation (CCA). However, very few EIICS calculations using these latter two methods are available, particularly at higher incident energies, where the quantum electrodynamical correction to the electron-electron interaction becomes significant. On the other hand, the understanding of the physical processes mentioned in the first paragraph requires the data or reliable calculations of EIICS for many targets and at large energy ranges. Hence, much effort has been made to develop simple phenomenological models for this purpose which can easily be incorporated in various codes dealing with the analyses of data associated with various processes mentioned earlier.

A variety of empirical models has been proposed to describe the electron-impact ionization process [2–8]. Each of these models seems to have some validity in a limited incident energy range or for a few targets but there is yet to be developed a model that works well at all incident energies and for many atomic targets. For example, the semi-empirical model of Green and Coslett [9] works well at low incident energies but appears to be inadequate to describe EIICS at reduced energies, $U = T/I \geq 4$, with T and I being the incident kinetic energy and ionization potential. Similarly, the model developed by Quarles [10] seems to work well for a limited number of atomic targets up to five orders in the value of U. In general, there seem to be a need to develop a model for high incident energies, where the relativistic correction becomes significant, but the model must also reproduce the observed data near

[a] e-mail: mauddin@ru.ac.bd

threshold region, particularly the shape and magnitude of the data in the peak region of cross-sections, Attempts to achieve this by Casnati et al. [3], Hombourger [4], and Deutsch et al. [5,6] have, so far, met with a limited success.

Kolbensvedt [11], in his attempt to find a suitable method for calculating EIICS, has proposed a model by combining the distant and close contributions to the collision cross-sections. According to the model, the contribution of σ_{ph} from distant collisions is due to an exchange of virtual photons between the incident and target electrons leading to ionization by the photoelectric effect. On the other hand, the cross-section σ_M from close collisions is contributed from the Møller interaction [12] incorporated in the impulse approximation. The model has been applied successfully to the description of K-shell ionization of silver and tin at incident energies much higher than the K-shell ionization potential. The model, however, usually overestimates the cross-sections from the threshold to peak region of cross-section and underestimates them at ultra high energies, albeit doing well in the moderately high energies. We have attempted, in this paper, to modify it in such a way as to fit data over the entire energy domain from low to relativistic energies. In an attempt to do so, we note that the contribution of σ_{ph} part of it, which dominates the ionization cross-section near threshold, is very large in comparison to the contribution of σ_M in the low energy region. It is the contribution from σ_{ph} that is responsible for abnormally high cross-sections in the region. We, therefore, propose to modify the behaviour of the σ_{ph} part at the low energy region first by modifying the energy denominator of the first term in its expression, akin to the modification done in [16] and then introduce an energy-dependent overall multiplicative factor. To account for the proper relativistic contribution to the cross-section, we suggest another term as a multiplying factor to the total Kolbensvedt cross-section, the sum of σ_{ph} and σ_M. The model, so framed, is henceforth referred to as the modified Kolbensvedt model with the acronym MKLV and that for the original Kolbensvedt model as KLV.

We apply MKLV to obtain the K-shell EIICS of neutral atoms and ions, for a number of targets from hydrogen to uranium at incident energies in the range $1 \leq U < 10^5$. To assess the efficacy of MLKV, we compare its predictions with the calculations of some empirical models including those of Casnati et al. (EMPC) [3], Hombourger (EMPH) [4] and Deutsch et al. (DM) [5], and the results of ab-initio quantum mechanical methods. The ranges of Z and incident energies, considered in this work, are wider than those investigated in [3–5].

The paper is organized as follows. Section 2 provides the outline of the MKLV model along with the underlying principles. Section 3 contains the results and discussion. In the discussion section, the results of the MKLV model are finally compared to the ab-initio calculations done in relativistic plane wave Born approximation with the Møller interaction. A summary of conclusions is given in Section 4.

2 Outline of the modified Kolbensvedt model

The total K-shell EIICS in the Kolbensvedt model [11] is given by

$$\sigma_{KLV} = \sigma_M(p < a) + \sigma_{ph}(p > a). \tag{1}$$

Here p is the impact parameter and a is the K-shell radius.

The two components σ_M and σ_{ph}, in the practical form, are

$$\sigma_M(p < a) = \frac{0.99}{I_K}\frac{(T+1)^2}{T(T+2)} \times \left[1 - \frac{I_K}{T}\left(1 - \frac{T^2}{2(T+1)^2} + \frac{2T+1}{(T+1)^2}\ln\frac{T}{I_K}\right)\right] \text{barns}, \tag{2}$$

and

$$\sigma_{ph}(p > a) = \frac{0.275}{I_K}\frac{(T+1)^2}{T(T+2)} \times \left[\ln\frac{1.19T(T+2)}{I_K} - \frac{T(T+2)}{(T+1)^2}\right] \text{barns}. \tag{3}$$

Here the incident energy T and the binding energy I_K of the K-shell are expressed in natural unit, i.e. in terms of electron rest mass energy. As mentioned earlier, the cross-sections in the low energy region is mainly from the σ_{ph} part arising from the contribution of the exchange of photons between the two colliding electrons. To ameliorate the low-energy deficiencies of KLV, we propose two modifications which are as follows:

(i) we introduce a multiplying factor F_M to σ_{ph};
(ii) we scale down the denominator $T(T + 2)$ in equation (3) taking into account the shielding of the incident and bound electrons by other electrons and ionic effect.

The F_M factor, following the work of Scott et al. [13], is used to trim the abnormally high values of the cross-section in the low energy region. Three alternative forms of the factor, suggested in [13], are: $F_M = aE^2$, $F_M = aE^{3/2}$ and $F_M = a\exp(11.9E^{-1/6})$ with $a = 0.00658$ and $E = T - I_K$. None of the above-mentioned forms produce the results in conformity with experiments. However, $F_M = a(1 - 1/U)$, which is close to the first two terms in the expansion of the exponential term of the third alternative, generates good fits to the experimental data at low energies. On the other hand, at higher energies, the factor F_M is not needed to modulate the σ_{ph} part of cross-sections as this part itself reproduces the experimental values. The values of the parameter a and the range of energy for application of F_M are obtained from the overall comparison of the calculated values with the experimental data for all the targets considered herein and others not mentioned for the sake of space. The aforesaid analysis results in the following expression for the multiplicative factor:

$$\begin{aligned} F_M &= 2.5(1 - 1/U) && \text{for } U \leq 1.70, \\ &= 1.0 && \text{for } U > 1.70. \end{aligned} \tag{4}$$

To achieve a further reduction in the magnitude of σ_{ph}, we seek to replace the denominator $T(T+2)$ in equation (3) considering the following points:

(a) in the binary-encounter Bethe (BEB) model of Kim and Rudd [14], the effective energy seen by a bound electron is not merely T, as in ab initio theories, but is $T + K + I_K$, K being the kinetic energy of the K-shell electron. This sort of correlation between the bound and incident electrons is needed to reduce the cross-sections in the low energy region, as demanded by experiments;
(b) the interaction between the incident and K-shell electron is that between a free electron and a bound one. The incident electron, as it approaches a K-shell electron in a neutral atom, sees it as an ion of charge $q = Z - 2$ except for hydrogen where $q = 0$. For an ionic target, the incident electron's path is governed by the ionic charge well before the encounter and as such q is set as the ionic charge.

The KLV model does not distinguish between the collision with a neutral atom and that with an ion in so far as the incident electron is concerned. The target electron description differs by I_K only. The electron approaching the K-shell electron feels an attractive force of the nucleus in a much greater magnitude than that experienced during its encounter with the valence-shell. Qualitatively, the charge cloud of the incident electron is attracted towards the nucleus, thereby increasing the overlap between the charge densities of the incident and bound electrons. This results in an enhancement of cross-sections. To incorporate appropriately the combined effects of the correlation and ionic effects, the scaling down of the denominator $T(T+2)$ in equation (3) is effected following the procedure of Kim [15]. In the latter, it has been shown that the calculated EIICS of H-like ions agrees well with experiments if $T+K+I_K$ is replaced by $T+(K+I_K)/(q+1)$. The σ_{ph} part in the KLV model bears some similarity in structure with the BEB model. Hence we have been tempted to implement the above replacement in modifying the model. However, a better performance has been obtained through the replacement of T by

$$T' = T + \frac{(K + I_K)}{0.5(q+1)^{1/2}}. \tag{5}$$

In line with [16] in connection with the Burgess denominator, we replace T by T' only in the denominator $T(T+2)$ of equation (3). Thus, the modified σ_{ph} becomes

$$\sigma''_{ph} = F_M \sigma'_{ph}. \tag{6}$$

Here, σ'_{ph} is obtained from σ_{ph} by replacing the denominator $T(T+2)$ by $D_C = T'(T'+2)$ in equation (3).

As will be evident from the calculations shown later in Figures 9–13, the KLV model fails to reproduce the experimental cross-sections at ultrarelativistic region of incident energies. Deutsch et al., in their DM model [5], used an additional relativistic correction factor $R_C = 1+2U^{1/4}/J^2$ (where $J = m_e c^2/I_K$ with m_e and c are, respectively, the rest-mass of electron and the velocity of light in vacuum) in conjunction with the Gryzinski's relativistic factor [17] to account for the inner-shell ionization cross-sections of atoms in the high energy region. The factor, however, does not work well in the structure of KLV. We have, therefore, looked for a suitable factor similar to the R_C factor, which can describe the experimental data well at all energy regions. Our suggested form of the factor is

$$R_F = (1 + mU^n). \tag{7}$$

The parameters m and n are determined from fits to the experimental data on many targets including those considered and those not mentioned herein. The optimum values of m and n are $m = 0.054$ and $n = 0.067$. In the light of the aforesaid arguments, the cross-section expression in the proposed MKLV model is given by

$$\sigma_{MKLV} = (F_M \sigma'_{ph} + \sigma_M) R_F. \tag{8}$$

3 Results and discussion

The K-shell binding energies of the neutral targets are taken from Desclaux [18]. The binding energies of ionic targets and kinetic energies of the K-shell electrons of all targets are calculated using the Dirac-Hartree-Fock code [19]. The radii of the maximum charge density of the orbit for neutral targets, as required in the DM model, are taken from [18] and those for the helium-like ions are calculated using the hydrogen-like wave function with the effective charge $Z_{eff} = Z - 5/16$ [20,21]. For the hydrogenic ions, the radius is obtained as $r = (1.15/Z^{1.05})a_0$ [22], a_0 being the Bohr radius.

In Figures 1–14, we compare the predicted EIICS from the MKLV model with the available experimental data and other theoretical results. The latter include the EIICS calculations from the models of Casnati et al. [3], Hombourger [4] and Uddin et al. [23,24], the DWBA calculations of Younger [25] and those from the relativistic DWBA (RDWBA) theory of Segui et al. [1] and perturbation method with exchange effect (PMEX) of Luo and Joy [26]. Elaborate sources of experimental EIICS data are Tawara and Kato [30] for ionic targets and Liu et al. [31] for neutral atoms. The experimental data are taken from Shah et al. [27], Peart and Dolder [28], Lineberger et al. [29], Aichele et al. [32], Donets and Ovsyannikov [33], Kamiya et al. [34], Ishii et al. [35], McDonald and Spicer [36], Hoffmann et al. [37,38], Hink and Ziegler [39], Quarles and Semaan [40], Platten et al. [41], Hippler et al. [42], Tawara et al. [43], Llovet et al. [44], Luo et al. [45], Shima [46], Scholz et al. [47,48], Zhou et al. [49], Middleman et al. [50], Schlenk et al. [51], Seif et al. [52], Ricz et al. [53], Davis et al. [54], Genz et al. [55], Rester and Dance [56], and Kiss et al. [57].

As expected, the calculations done using the KLV model usually overestimates EIICS from the threshold to peak region for targets considered herein, except for Al. The model, in general underestimates the observed cross-sections at incident energies higher than 2 MeV for Mn,

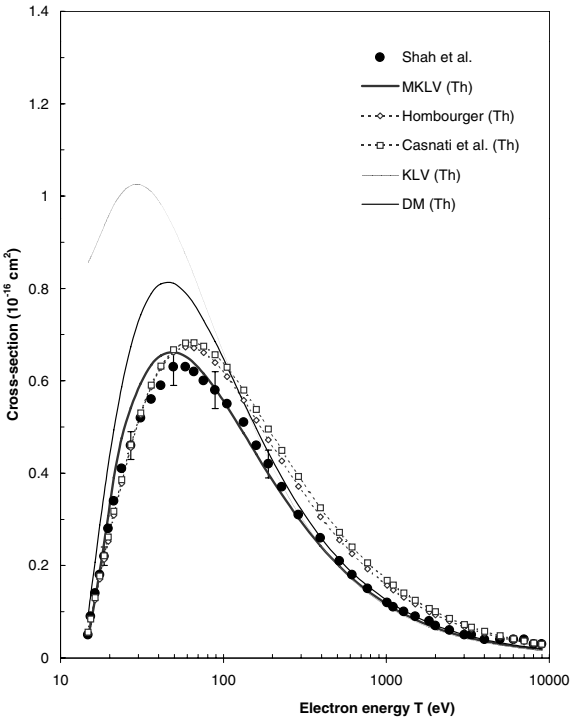

Fig. 1. Electron impact K-shell ionization cross-sections for H. Solid circles are the experimental data from [27]. The shaded, thick solid, thin solid, broken line with open squares and broken line with open diamonds are the present calculations using, respectively, the KLV [11], proposed MKLV, DM models and the empirical models of Casnati et al. [3] and Hombourger [4]. All the theoretical predictions are marked by (Th) in legends.

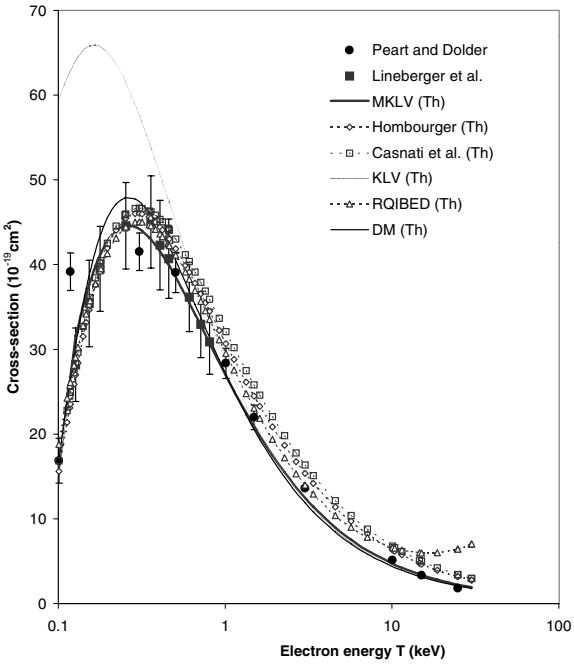

Fig. 2. Same as in Figure 1 for Li^+. The experimental data are solid circles from [28] and solid squares from [29]. The broken line with open triangles are the calculations from the RQIBED model of [23].

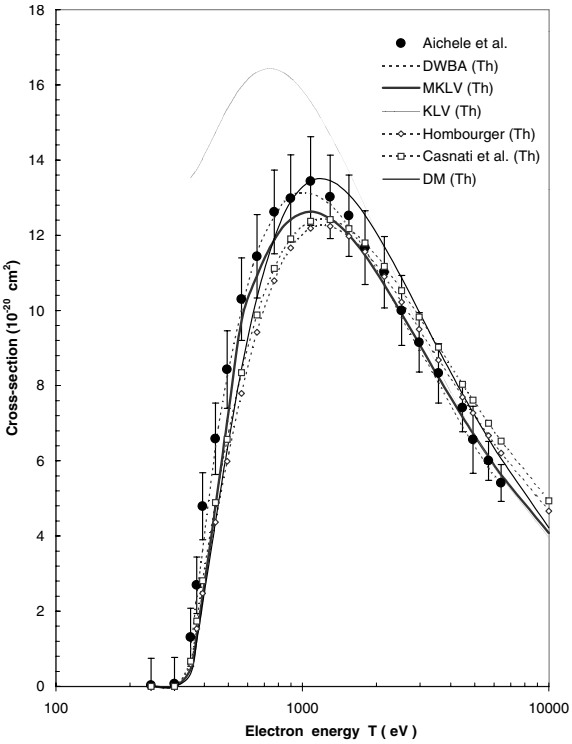

Fig. 3. Same as in Figure 1 for B^{4+}. The experimental data are the solid circles from [32]. The broken curve denotes the DWBA calculations of Younger [25].

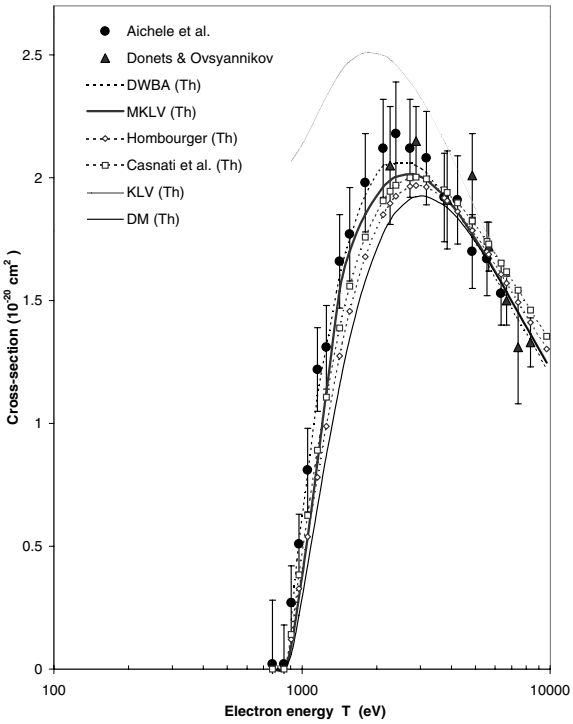

Fig. 4. Same as in Figure 3 for O^{7+}. The solid triangles are the experimental data from [33].

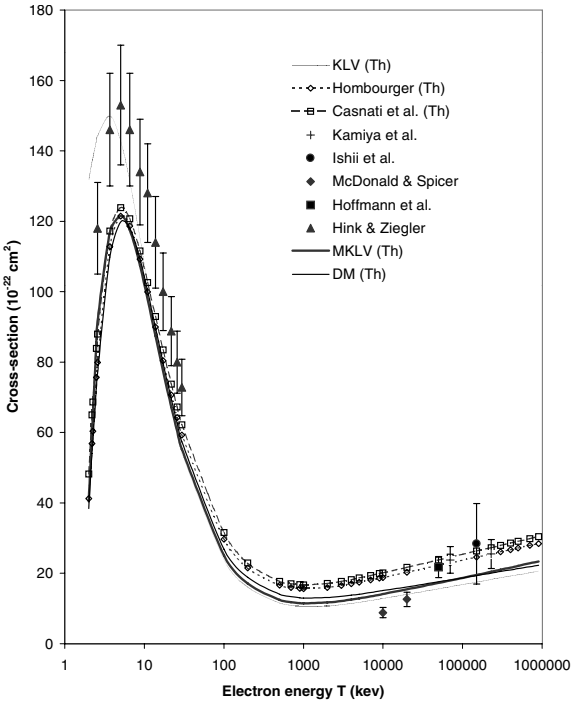

Fig. 5. Same as in Figure 1 for Al. The experimental data are pluses from [34], solid circles from [35], solid diamonds from [36], solid squares from [37,38] and solid triangles from [39].

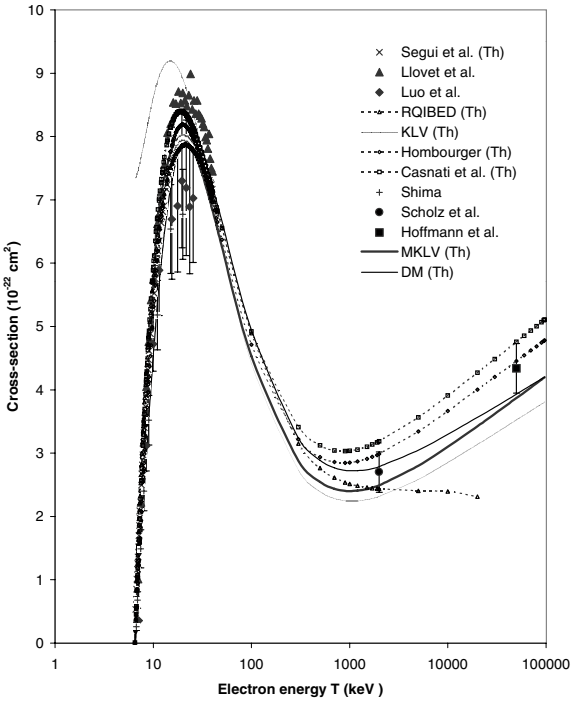

Fig. 7. Same as in Figure 6 for Mn. The experimental data are solid squares from [37,38], solid triangles from [44], solid diamonds from [45], solid circles from [47,48] and pluses from [46].

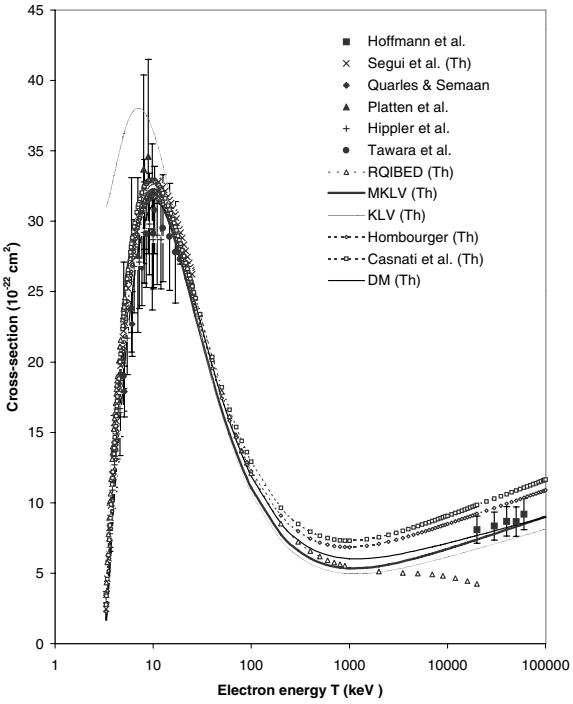

Fig. 6. Same as in Figure 1 for Ar. The experimental data are solid squares from [37,38], solid diamonds from [40], solid triangles from [41], solid circles from [43] and pluses from [42]. The broken curve with open triangles are the results from the RQIBED model of [23]. The crosses are the relativistic DWBA calculations of Segui et al. [1].

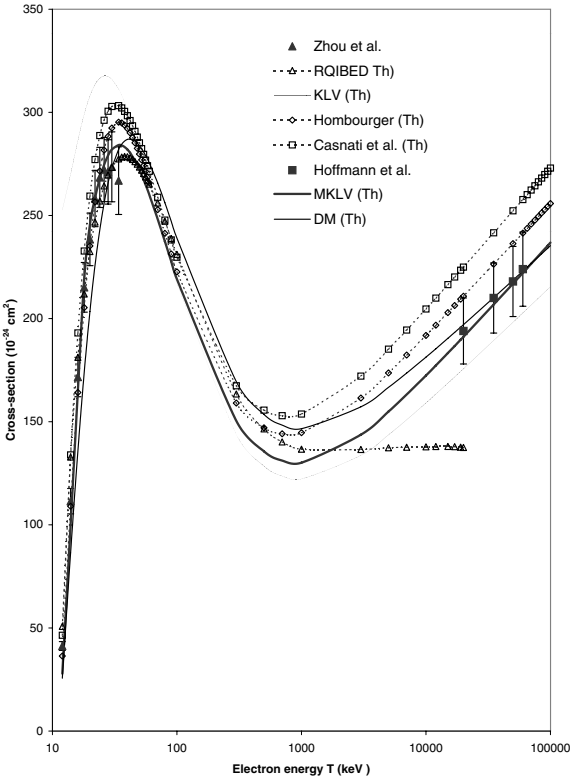

Fig. 8. Same as in Figure 2 for Ge. The experimental data are now solid squares from [37,38] and solid triangles from [49].

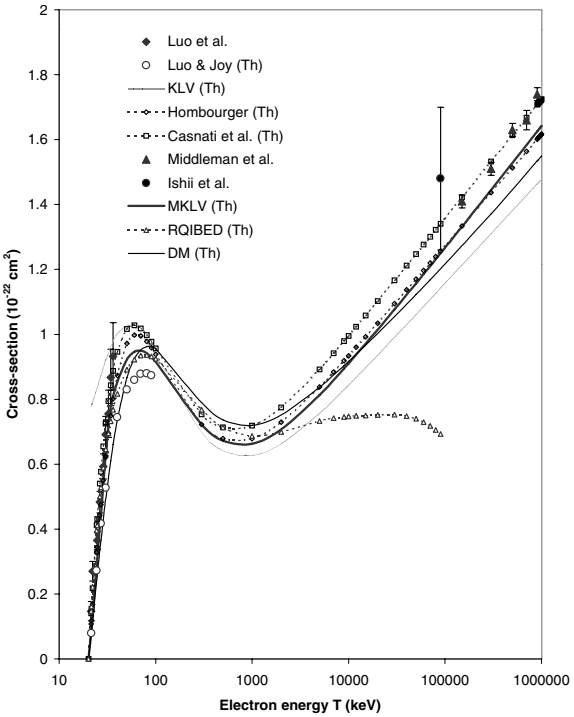

Fig. 9. Same as in Figure 2 for Mo. The experimental data are now solid circles from [35], solid diamonds from [45] and solid triangles from [50]. The open circles are the perturbation calculations of Luo and Joy [26].

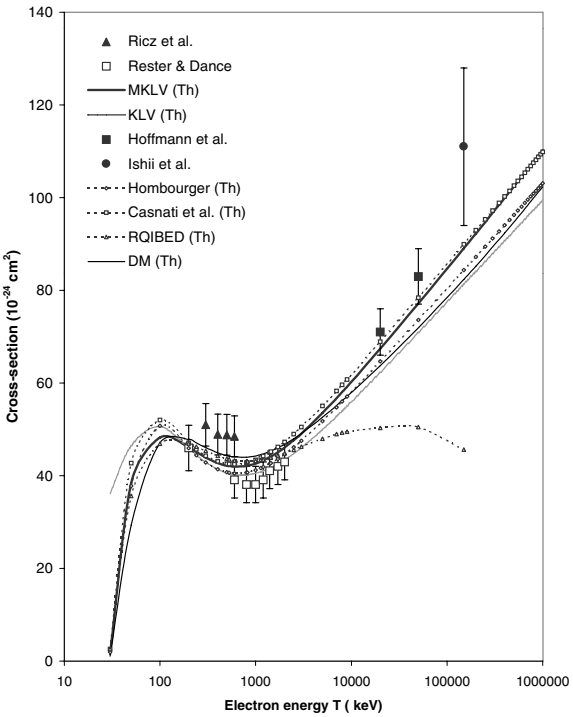

Fig. 11. Same as in Figure 2 for Sn. The experimental data are now solid circles from [35], solid squares from [37,38], and solid triangles from [53] and open squares from [56].

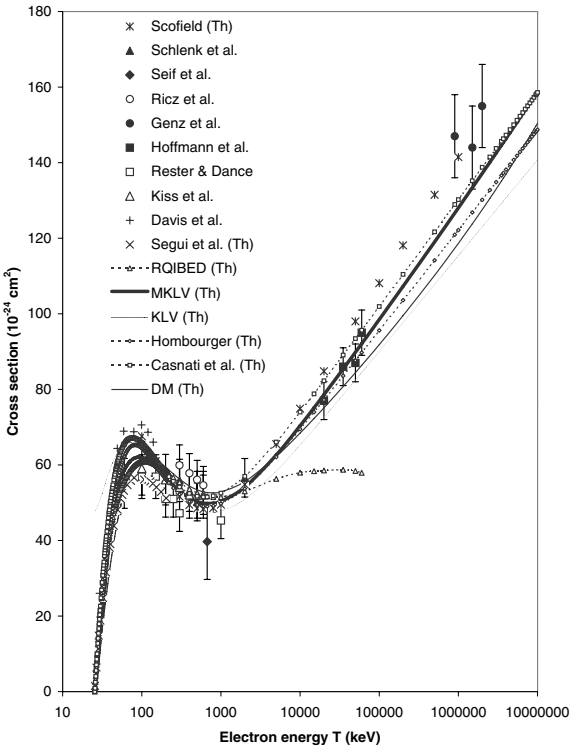

Fig. 10. Same as in Figure 6 for Ag. The experimental data are now solid squares from [37,38], solid triangles from [51], solid diamonds from [52], solid circles from [55], open circles from [53], pluses from [54], open squares from [56], open triangles from [57] and asterisks from [58].

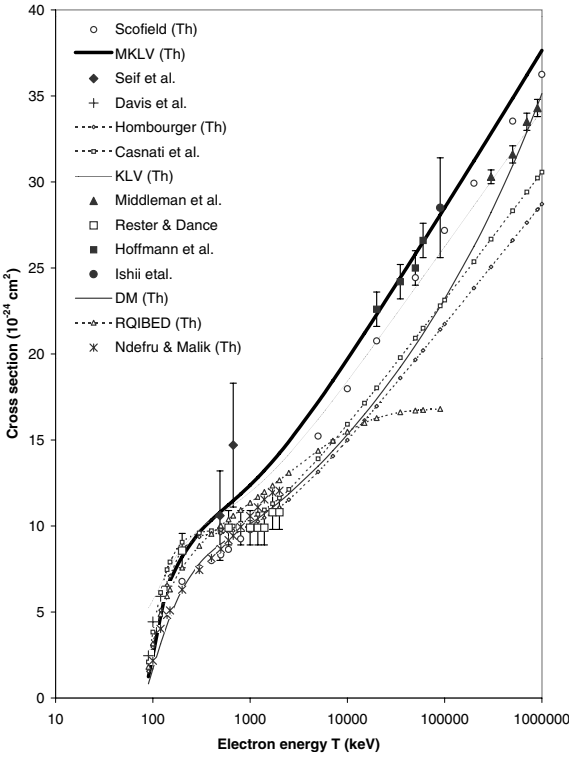

Fig. 12. Same as in Figure 2 for Au. The experimental data are now solid circles from [35], solid squares from [37,38], solid triangles from [50], solid diamonds from [52], pluses from [54], open squares from [56], open circles from [58] and asterisks from [59].

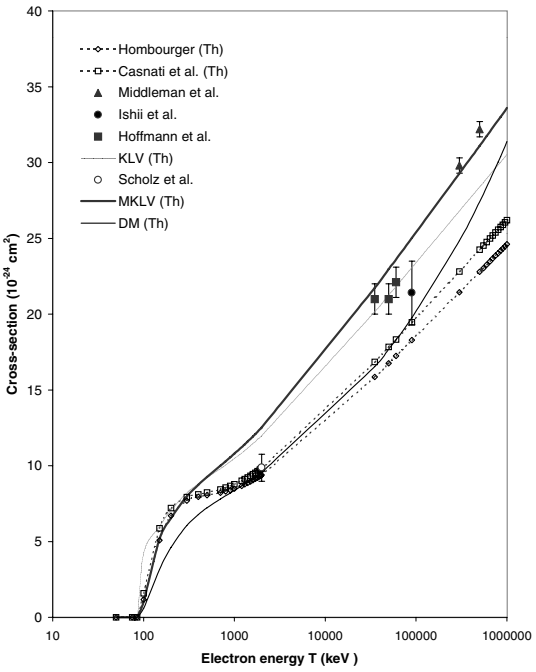

Fig. 13. Same as in Figure 1 for Bi. The experimental data are now solid squares from [37,38], solid circles from [35] pluses from [48] and solid triangles from [50].

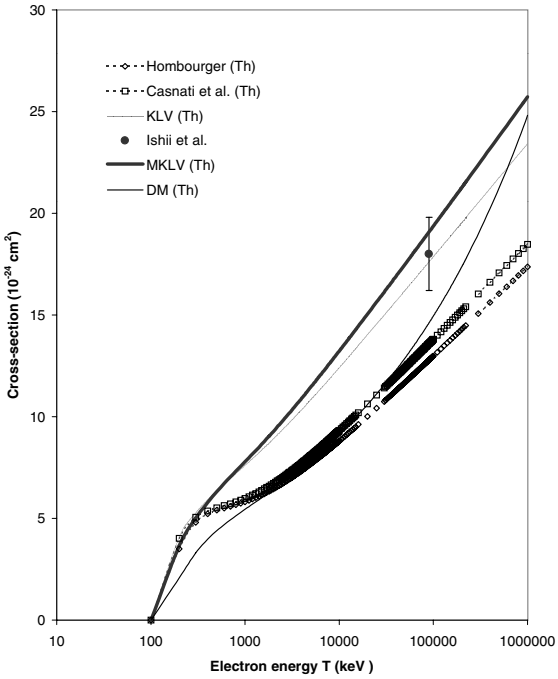

Fig. 14. Same as in Figure 1 for U. The experimental data are now solid circles from [35].

10 MeV for Ge, 20 MeV for Mo, 200 MeV for Ag, and 100 MeV for Sn and Bi. However, the data for Au are well accounted for by the KLV model in the entire energy interval.

The K-shell ionization cross-sections calculated using the empirical models, EMPC of Casnati et al. [3] and EMPH of Hombourger [4], are also presented for these targets in Figures 1–14. They are supposed to be valid for $6 \leq Z \leq 79$. In general, these calculations are close to the ones done in the MKLV model from the threshold to peak region, but tend to overestimate the cross-sections for H. The calculations done using EMPC and EMPH differ significantly from those done using the MKLV model at higher energies and do not account for the data very well, particularly for the Ge, Au, Bi and U targets.

The predicted EIICS values from the RQIBED model [23,24] for Li^+, Ar, Mn, Ge, Mo, Ag, Sn and Au are compared with the experimental data and other theoretical results in Figures 2, 6–12. The RQIBED predictions agree closely with the experimental data and/or the calculations using the MKLV, EMPC and EMPH models up to about 10 keV for Li^+; about 1 MeV for Ar, Mn and Ge; about 3 MeV for Mo and Ag; and about 5 MeV for Sn and Au.

Deutsch et al. have incorporated a relativistic correction to their earlier model in [5] and calculations based on their model, termed as DM, have been presented in each case. The calculations done using the DM model overestimate the cross-sections of H around the peak region (Fig. 1). The model produces satisfactory fit to the experimental data of Li^+ (Fig. 2), and reasonable fits to the data of B^{4+} (Fig. 3) and O^{7+} (Fig. 4). For the Al target, the DM model underestimates the cross-sections in the peak regions but generates good fits to the data at the higher energies (Fig. 5). The model accounts for the data of Ar (Fig. 6) very well and those of Mn (Fig. 7) and Ge (Fig. 8) satisfactorily thoughout the entire energy domain. Although the calculations done using the DM model do well at lower energies, it fails to reproduce the data in the 100–900 MeV energy region in the case of Mo (Fig. 9) and the data at energies higher than 1000 MeV for Ag (Fig. 10). For Bi (Fig. 13) and U (Fig. 14), the experimental EIICS data at incident energies higher than 100 MeV could not be reproduced by the model.

In the overall picture, the calculations done in the MKLV model account for the data better than those obtained by the other empirical models discussed above. The inadequacy of the KLV model to reproduce the data near the threshold and peak region is corrected, in the MKLV model, by changing the denominator $T(T+2)$ in equation (3) to D_C and then introducing the multiplying factor F_M to σ'_{ph}. At higher energies, where the σ_M part of the cross-section dominates, the underestimation of the observed cross-sections in the KLV model is corrected by incorporating the overall multiplicative factor R_F. The calculations of the MKLV model describe the data near the threshold and in the peak region very well, except for Al where, like all other calculations, the results of the MKLV model underestimate the magnitude of the peak cross-sections slightly but reproduce well the shape and the width. The calculated cross-sections in the MKLV model at higher energies, in general, reproduce the data for each target with three notable exceptions, viz. the calculations seem to underestimate slightly the data around 200 MeV for Sn and 500–900 MeV for Mo, and overestimate around 800–1000 MeV for Au. However, the calculated results,

in each case, lie within 10% of the data. The calculations using the models of [3–5], in general, produce lower cross-sections compared to those predicted by the MKLV model for the Au, Bi and U targets and do not account for the data.

Because of the success of the MKLV model in accounting for the data from the threshold region to very high energies for many targets, it is of interest to compare its results with the ab-initio quantum mechanical calculations. The DWBA results of [25] for B^{4+} (Fig. 3) and O^{7+} (Fig. 4) agree closely with the experimental EIICS and the MKLV predictions. The RDWBA cross-sections of [1] for Ar up to about 25 keV (Fig. 6), Mn up to about 40 keV (Fig. 7), and Ag up to about 200 keV incident energies (Fig. 10) follow closely the predicted values from the present MKLV model. The PMEX calculations of [26] for Mo (Fig. 9) underestimate the experimental data in the peak region up to about 100 keV. The calculations done using the MKLV model follow the results of ab-initio predictions closely in these energy ranges and explain the data equally well.

Scofield [58] has performed detailed relativistic plane wave calculations using (a) the normalized plane wave solutions of the Dirac equation, (b) the Møller interaction between the incident electron and the colliding K-shell electron, and (c) the mean field perceived by the K-shell electron in the Dirac-Hartree-Fock-Slater approximation for the elements with Z = 18, 28, 39, 47, 56, 67, 79, 83 and 92 in the incident energy range of 0.05 to 1000 MeV. His calculations using the relativistic plane-wave Born approximation with the Møller interaction, termed here as RPBM-S, explain the data above 0.1 MeV incident energy for Ag (Fig. 10) and 1 MeV incident energy for Au (Fig. 12) well but not near the threshold and in the peak region. The results attained in the MKLV model follow his calculations closely in 3 to 1000 MeV region but also account for the data at lower energies. Scofield's predictions for cross-sections of 1072, 23.53 and 17.19 barns, respectively, for Ar at 50 MeV, Bi at 100 MeV and U at 100 MeV are close to the experimental results and to the calculations done in the MKLV model.

Ndefru and Malik [59] performed calculations, referred to here as RPBM-NM, from the threshold to 2 MeV incident energies for Au (Fig. 12) using the relativistic plane-wave Born approximation with the Møller interaction, similar to the one of Scofield, except that the exchange between the two electrons were included in their calculations. The data around 2 MeV are reproduced somewhat better by them compared to the calculations of Scofield and the MKLV model. Nevertheless, the difference may not be significant in view of the large error bars accompanying the data.

Ndefru, Wills and Malik [60] performed calculations using the theory of [58] for a number of elements from Sn to Pb at 2 MeV incident electrons and except for Ni, explained the data well. The calculations done in the MKLV model at this energy for Sn, Ag, Au and Bi are close to the relativistic calculations of [60].

Thus, the calculations done in the MKLV model closely follow most of the calculations done in relativistic Born approximation using the Møller interaction at incident energies higher than a tenth of a MeV, and at the same time explain the data in the peak region of cross-sections.

4 Conclusions

Of all the empirical models considered herein, the overall agreement to the data is best achieved by the calculations using the MKLV model proposed in this article. The calculated results in the MKLV model also reproduce closely the ab-initio calculations done by Scofield [58] and Ndefru and Malik [59] for the Au target and by Scofield for the Ag target at energies above the peak region. At lower energies, the results of RPBM-S and RPBM-NM underestimate the data somewhat, but the MKLV calculations can account for the data.

The results of the proposed MKLV model are very encouraging in successfully explaining the data for a wide range of targets and incident energies. The method, with its root in the quantum electro-dynamical treatment of two-electron potential, can explain the data in this article within 10%.

The authors are thankful to Dr. A.S.B. Tariq of Rajshahi University for his valuable comments.

References

1. S. Segui, M. Dingfelder, F. Salvat, Phys. Rev. A **67**, 062710 (2003)
2. C.J. Powell, *Electron Impact Ionization*, edited by T.D. Märk, G.H. Dunn (Springer-Verlag, Berlin, 1985)
3. E. Casnati, A. Tartari, C. Baraldi, J. Phys. B: At. Mol. Phys. **15**, 155 (1982)
4. C. Hombourger, J. Phys. B: At. Mol. Phys. **31**, 3693 (1998)
5. H. Deutsch, D. Margreiter, T.D. Märk, Z. Phys. D **29**, 31 (1994)
6. H. Deutsch, K. Becker, B. Gstir, T.D. Märk, Int. J. Mass Spectrom. **213**, 5 (2002)
7. Y.-K. Kim, J.P. Santos, F. Parente, Phys. Rev. A **62**, 052710 (2001)
8. C.-H. Tang, Z. An, X.-Q. Fan, Z.-M. Luo, Chin. Phys. Lett. **18**, 1053 (2001)
9. M. Green, V.E. Coslett, Proc. Phys. Soc. (London) **78**, 1206 (1961)
10. C.A. Quarles, Phys. Rev. **13**, 1278 (1975)
11. H. Kolbensvedt, J. Appl. Phys. **38**, 4785 (1967)
12. C. Møller, Z. Phys. **70**, 786 (1931)
13. M.P. Scott, P.G. Burke, K. Bartschat, I. Bray, J. Phys. B: At. Mol. Phys. **30**, L309 (1997)
14. Y.-K. Kim, J.P. Santos, F. Parente, Phys. Rev. A **50**, 3954 (1994)
15. Y.-K. Kim, Phys. Essays **13**, 473 (2000)
16. M.A. Uddin, A.K. Basak, A.K.M.A. Islam, F.B. Malik, J. Phys. B: At. Mol. Opt. Phys. **37**, 1909 (2004)
17. M. Gryzinski, Phys. Rev. **138**, 322 (1965)

18. J.P. Desclaux, At. Nucl. Data Tables **12**, 325 (1973)
19. M.Y Amusia, L.V. Chernysheva, *Computations of Atomic Processes* (Institute of Physics Publishing, Bristol, 1997).
20. M.F. Gadi, P. Defrance, A. Makhute, M.H. Cherkani, Phys. Scripta **63**, 462 (2001)
21. M.A. Uddin, A.K. Basak, B.C. Saha, Int. J. Quant. Chem. **100**, 184 (2004)
22. H. Deutsch, K. Becker, T.D. Märk, Nucl. Instr. Meth. Phys. Res. B **98**, 135 (1995)
23. M.A. Uddin, M.A.K.F. Haque, A.K. Basak, B.C. Saha, Phys. Rev. A **70**, 032706 (2004)
24. M.A. Uddin, A.K.F. Haque, A.K. Basak, K.R. Karim, B.C. Saha, Phys. Rev. A **71**, 032715 (2005)
25. S.M. Younger, J. Quant. Spectrosc. Radiat. Transfer **26**, 329 (1981)
26. S. Luo, D.C. Joy, *Microbeam analysis*, edited by D.G. Howitt (Sanfrancisco Press, San Francisco, CA, 1991), p. 67
27. M.B. Shah, D.S. Elliott, H.B. Gilbody, J. Phys. B: At. Mol. Opt. Phys. **20**, 3501 (1987)
28. B. Peart, K.T. Dolder, J. Phys. B: At. Mol. Opt. Phys. **1**, 872 (1968)
29. W.C. Lineberger, J.W. Hooper, E.W. McDaniel, Phys. Rev. **141**, 151 (1966)
30. H. Tawara, T. Kato, At. Data Nucl. Data Tables **36**, 167 (1987)
31. M. Liu, Z.A.C. Tang, Z. Luo, X. Peng, X. Long, At. Data Nucl. Data Tables **76**, 213 (2000)
32. K. Aichele et al., J. Phys B: At. Mol. Opt. Phys. **31**, 2369 (1998)
33. E.D. Donets, V.P. Ovsyannikov, Sov. Phys.-JEPT **53**, 466 (1981)
34. M. Kamiya, A. Kuwako, R. Ishii, S. Morita, H. Oyamada, Phys. Rev. A **22**, 413 (1980)
35. R. Ishii, M. Kamiya, K. Sera, S. Morita, H. Tawara, H. Oyamada, T.C. Chu, Phys. Rev. A **15**, 906 (1977)
36. S.C. McDonald, B.M. Spicer, Phys. Rev. A **37**, 985 (1988)
37. D.H.H. Hoffmann, H. Genz, W. Low, A. Richter, Phys. Lett. **65A**, 304 (1978)
38. D.H.H. Hoffmann, C. Brendal, H. Genz, W. Low, S. Muller, A. Richter, Z. Phys. A **293**, 187 (1979)
39. W. HinK, A. Ziegler, Z. Phys. **226**, 222 (1969)
40. C. Quarles, M. Semaan, Phys. Rev. A **26**, 3147 (1982)
41. H. Platten, G. Schiwietz, G. Nolte, Phys. Lett. **107A**, 83 (1985)
42. R. Hippler, K. Saeed, I. McGregor, H. Kleimpoppen, Z. Phys. A **307**, 83 (1982)
43. H. Tawara, K.G. Horrison, F.G. de Heer, Physica **63**, 351 (1973)
44. X. Llovet, C. Merlet, F. Salvat, J. Phys. B: At. Mol. Phys. **33**, 3761 (2000)
45. Z.M. Luo, Z. An, F.Q. He, T. Li, X.G. Long, X.F. Peng, J. Phys. B: At. Mol. Phys. **78**, 4001 (1996)
46. K. Shima, Phys. Lett. A **77**, 237 (1980)
47. W. Scholz, A. Li-Scholz, R. Collé, I.L. Preiss, Phys. Rev. Lett. **29**, 761 (1972)
48. A. Li-Scholz, R. Collé, I.L. Preiss, W. Scholz, Phys. Rev. A **7**, 1957 (1973)
49. C. Zhou, Z. An, Z. Luo, J. Phys. B: At. Mol. Phys. **35**, 841 (2002)
50. L.N. Middleman, R.L. Ford, R. Hofstadter, Phys. Rev. A **2**, 1429 (1970)
51. B. Schlenk, D. Berenyl, S. Ricz, A. Valek, G. Hock, Acta Phys. Hung. **41**, 159 (1976)
52. S.A.H. Seif el Naser, D. Berenyl, G. Bibok, Z. Phys. **267**, 169 (1974)
53. S. Ricz, B. Schlenk, D. Berenyl, G. Hock, A. Valek, Acta Phys. Hung. **42**, 269 (1977)
54. D.V. Davis, V.D. Mistry, C.A. Quarles, Phys. Lett. **A38**, 169 (1972)
55. H. Genz, C. Brendal, P. Eschwey, U. Kuhn, W. Low, A. Richter, P. Seserko, Z. Phys. **305**, 9 (1982)
56. D.H Rester, W.E. Dance, Phys. Rev. **152**, 1 (1966)
57. K. Kiss, Gy. Kalman, J. Palinkas, B. Schlenk, Acta Phys. Hung. **50**, 97 (1981)
58. J.H. Scofield, Phys. Rev. A **18**, 963 (1978)
59. J.T. Ndefru, F.B. Malik, Phys. Rev. A **25**, 2407 (1982)
60. J.T. Ndefru, J.G. Wills, F.B. Malik, Phys. Rev. A **21**, 1049 (1980)